Arch. Metall. Mater. **64** (2019), 1, 329-338

DOI: 10.24425/amm.2019.126256

T. DOMAŃSKI*#

NUMERICAL ANALYSIS OF THERMO-MECHANICAL PHENOMENA OF THE PROGRESSIVE HARDENING ELEMENTS MADE OF TOOL STEEL FOR COLD WORK

The numerical algorithm of thermal phenomena is based on the solution of the heat conduction equations in Petrov-Galerkin's formula using the finite element method. In the modeling of phase transformation in the solid state, the models based on the diagrams of continuous heating and continuous cooling (CHT and CCT). In the modeling of mechanical phenomena, equations of equilibrium and constitutive relationships were adopted in the rate form. It was assumed that the hardened material is elastic-plastic, and the plasticizing can be characterized by isotropic, kinematic or mixed strengthening. In the model of mechanical phenomena besides thermal, plastic and structural strains, the transformations plasticity was taken into account. Thermo-physical size occurring in the constitutive relationship, such as Young's modulus and tangential modulus, while yield point depend on temperature and phase composition of the material. The modified Leblond model was used to determine transformation plasticity. This model was supplemented by an algorithm of modified plane strain state, advantageous in application to the modeling of mechanical phenomena in slender objects. The problem of thermoelasticity and plasticity was solved by the FEM. In order to evaluate the quality and usefulness of the presented numerical models, numerical analysis of temperature fields, phase fractions, stresses and strains was performed, i.e. the basic phenomena accompanying surface layer of progressive-hardening with a movable heat source of slender elements made of tool steel for cold work.

Keywords: Hardening, strains, stresses, numerical analysis

1. Introduction

The variety of working conditions of tools creates the need to diversify the requirements for tool steels. The tool is always sought for the highest durability, and this is achieved by using appropriate heat treatment with a hardening procedure. The prediction of final properties of the element that undergoes progressive hardening is possible after defining the type of the formed microstructure, instantaneous stresses, and then of internal stresses that necessarily accompany this thermal treatment. In order to achieve this aim it is essential to consider such a treatment of thermal phenomena, phase transformations and mechanical phenomena in numerical modeling (Fig. 1). Phenomena that are complicated, and so far they are incompletely described. Findings of the numerical simulation of the above-mentioned phenomena depend on, inter alia, the accuracy of determination of phase transformation kinetics in the solid state [1-3]. To have the possibility to carry out a full analysis of thermal treatment it is necessary to have proper mathematical and numerical models that can provide information about instantaneous temperature fields, the change in time of fractions of particular phase proportions of the material, instantaneous stress distributions and, as a result, about internal stresses.

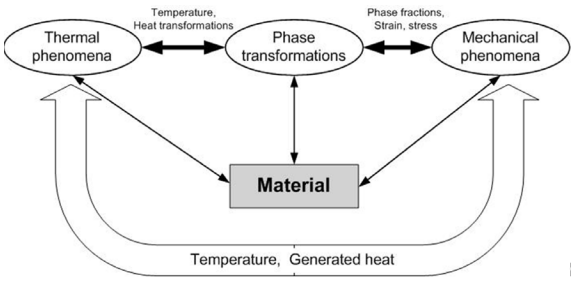

Fig. 1. Scheme of interdependence of thermo-mechanical phenomena of hardening

Numerical analysis of heat treatment processes is an important problem facing modern design studios for the industry, not necessarily steel. Particular accent on the development of this branch of numerical methods is inspired by the industry, which, due to modern technologies and efforts to reduce costs, is looking for tools to improve heat treatment processes [4-6]. Currently, the numerical analysis of thermal treatment processes is an important problem standing before contemporary workers designing for a given industry, not necessarily connected with steel. Special emphasis put on this branch of numerical methods is inspired by the industry that, due to modern technologies and

* CZESTOCHOWA UNIVERSITY OF TECHNOLOGY, FACULTY OF MECHANICAL ENGINEERING AND COMPUTER SCIENCE, INSTITUTE OF MECHANICS AND FUNDAMENTALS OF MACHINE DESIGN, 73 DĄBROWSKIEGO STR., 42-200 CZĘSTOCHOWA, POLAND

Corresponding author: domanski@imipkm.pcz.czest.pl

aims to reduce costs, requires tools improving thermal treatment processes [2,7-10]. The analysis of findings obtained by means of experimental research lead to the formation of many mathematical models that determine phase fractions in the solid state. The primary equations in almost all formulations pertaining to the transformation of austenite into ferrite, perlite and bainite are the Johnson-Mehl - Avrami equation [11]. To determine the fraction of the diffusionless phase, one may mainly use the Koistinen-Marburger equation or its modified versions [12]. The element that has a decisive influence on the numerical simulation findings pertaining to hardening is also connected with the proper selection of cooling conditions that are modeled with boundary conditions. Significant stresses are generated in the thermal treatment process. In order to ensure the credibility of numerical simulation findings of mechanical phenomena, one should also consider transformation plasticity in addition to thermal, structural and structural strains [3,5,9,13]. Up to now, there are no comprehensive numerical models regarding the hardening of the carbon tool steel group. Existing models are, to some extent, fragmentary. They most often pertain to phase transformations in the cooling process without a link to stresses that are generated in such processes.

For numerical modeling of heat treatment phenomena, the finite element method, the finite difference method, and less often the boundary element method are most often used [2,5,9]. The credibility of obtaining findings of numerical simulations often depends on the selection of a method of calculation, and it mainly pertains to the possibility of consideration, or non-consideration, of multiplicity of phenomena in the model, with respect to the hardening process. For this reason, the finite element method was used to solve thermal conduction problems and the problems of thermo-elasticity and plasticity.

2. Thermal phenomena

In the model of thermal phenomena of the progressive steel hardening process we used the conductivity equation with a convection term. Arguments of the sought-after temperature field are, spatial coordinates (Euler coordinates). This equation, which governs temperature distribution in the Ω area with a boundary $\Gamma = \Gamma_D \cup \Gamma_q \cup \Gamma_\infty$, has the following form [14]:

$$\nabla \cdot \left(\lambda \nabla T\left(x_\alpha, t\right)\right) - C_{ef} \frac{\partial T\left(x_\alpha, t\right)}{\partial t} + \\ - C_{ef}\, \mathbf{v}\left(x_\alpha, t\right) \cdot \nabla T\left(x_\alpha, t\right) = -\dot{Q}\left(x_\alpha, t\right), \; x_\alpha \in \Omega \qquad (2.1)$$

where: $T = T(x_\alpha,t)$ is the temperature [K], $\lambda = \lambda(x_\alpha)$ is the thermal conductivity coefficient [W/(mK)], $C_{ef} = C_{ef}(x_\alpha)$ is the proper effective heat capacity [J/(m^{3}K)], in which one may consider the heat of phase transformation (in a particular case it is equal to $C_{ef} = C = c\rho$, c – specific heat [J/(kgK)], ρ – density [kg/m^3], $\dot{Q} = \dot{Q}(x_\alpha,t$ is the capacity of internal sources [W/m^3], x_α is the position vector of the considered particle (point), $\mathbf{v} = \mathbf{v}(x_\alpha,t)$ [m/s] is the particle velocity vector in the control area of the considered object, t means time [s].

Equation (2.1) is supplemented with the initial and boundary conditions:

– initial conditions

$$T\left(x_\alpha, t_0\right) = T_0\left(x_\alpha\right), \\ \mathbf{v}\left(x_\alpha, t_0\right) = \mathbf{v}_0\left(x_\alpha\right), \\ \dot{Q}\left(x_\alpha, t_0\right) = \dot{Q}_0\left(x_\alpha\right) \qquad (2.2)$$

– boundary conditions

a) Temperature is given on the part of the boundary Γ_D, the Dirichlet condition (first-type condition). This condition type is given on one of the boundaries of the control area.

$$T\big|_{\Gamma_D} = T^*\left(x_\alpha\big|_{\Gamma_D}, t\right) \qquad (2.3)$$

b) Heat flux (q^*) on the part of the boundary Γ_∞ (intensive cooling zone) is determined by the temperature difference of the boundary and the surrounding medium, Newton Condition (third-type condition). In this work, such boundary condition is used to model cooling.

$$q = -\lambda \frac{\partial T}{\partial n}\bigg|_{\Gamma_\infty} = q^* = \alpha_\infty\left(T\right)\left(T\big|_{\Gamma_\infty} - T_w\right) \qquad (2.4)$$

where: $\alpha_\infty = \alpha_\infty(T)$ is the heat transfer coefficient [W/(m^{2}K)], T_w is the temperature of the cooling medium (ambient temperature from the side Γ_∞).

If on the part of the boundary Γ_∞ heat transfer depends on the intensity of radiation, then the heat flux (q^*) (in the Newton condition) is supplemented with the flux resulting from the intensity of radiation. In the numerical algorithm, we use the substitution [14]:

$$q = -\lambda \frac{\partial T}{\partial n}\bigg|_{\Gamma_\infty} = q^* = \alpha^*_\infty\left(T\right)\left(T\big|_{\Gamma_\infty} - T_\infty\right), \\ \alpha^*_\infty\left(T\right) = \alpha_r \sqrt[3]{T\big|_{\Gamma_\infty} - T_\infty} \qquad (2.5)$$

where: $\alpha^*_\infty = \alpha^*_\infty(T)$ is the heat transfer coefficient that includes convection as well as radiation, and α_r is the experimentally determined heat transfer coefficient.

Substitution of (2.5) allows us to retain the classical Newton condition in the numerical algorithm pertaining to the solution of the thermal conductivity problem. The finite element method in the formulation of Petrov-Galerkin was used to solve the above-mentioned problem of heat conductivity, i.e., the conductivity equation (2.1) with boundary conditions (2.3)÷(2.5). In the built algorithm, weight functions ($w = w(x_\alpha)$) are the so-called "upwind function" [14].

3. Phase transformations

In the model of phase transformations take advantage of diagrams of continuous heating (CHT) and cooling (CCT) [15,16]. Initial phase transformation in the austenite is a diffusive

transformation. The kinetics of transformation good defined the formula Johnson - Mehl - Avrami [11], i.e.:

$$\eta_A^H(T,t) = 1 - \exp(-b(t_s,t_f)\left(t^{n(t_s,t_f)}(T)\right) \qquad (3.1)$$

where: η_A^H is austenite initial fraction nascent in heating process, $b(t_s,t_f)$ and $n(t_s,t_f)$ are coefficients determined from the transformation (3.1) assuming the initial fraction ($\eta_s(t_s) = 0.01$) and final fraction ($\eta_f(t_f) = 0.99$) forming a phase, t_s and t_f are start times and end of transformations.

Pearlite and bainite fractions (in the model of phase transformations upper and lower bainite is not distinguish) are determined by Johnson-Mehl and Avrami formula, taking into account the fraction of the austenite phase formed in the heating process, i.e.:

$$\eta_{(\cdot)}(T,t) = \psi\left(1 - \exp\left(-bt^n(T)\right)\right),$$
$$\psi = \eta_{(\cdot)}^{\%}\eta_A^H \text{ for } \underline{\eta}_A \geq \eta_{(\cdot)}^{\%}$$
$$\text{and } \psi = \eta_A^H \text{ for } \eta_A^H < \eta_{(\cdot)}^{\%} \qquad (3.2)$$

where: $\eta_{(\cdot)}^{\%}$ is the maximum phase fraction for the established of the cooling rate, estimated on the based of the continuous cooling graph [16].

The fraction of martensite forming below the temperature M_s is determined by the Koistinen and Marburger formula [12]:

$$\eta_M(T) = \psi\left(1 - \exp\left(-k(M_s - T)^m\right)\right) \qquad (3.3)$$

where: m is the constant chosen by means of experiment (for considered steel determine m = 1), whereas the constant k is determined from (3.3) the end of transformation condition at the temperature M_f (for $\psi = 1$):

$$k = -\frac{\ln\left(1 - \eta\left(M_f\right)\right)}{M_s - M_f} = -\frac{\ln(0.01)}{M_s - M_f} \qquad (3.4)$$

With respect to considered steel, for which M_s = 493 K, $M_f \approx$ 173 K, the constant k resulting from (3.4) is equal to: k = 0,0144. The obtained coefficient is comparable to the value given in literature with respect to carbon near-eutectoid steels ($k \approx 0.011$) [9].

Increases of the isotropic strain ($\dot{\varepsilon}^{Tph}$) caused by changes of the temperature and phase transformation in the heating and cooling processes are calculated using the following relations for heating and cooling, respectively:

$$\dot{\varepsilon}^{Tph} = \dot{\varepsilon}_H^{Tph} = \sum_{k=1}^{k=5}\alpha_k\eta_k\dot{T} - \varepsilon_A^{ph}\dot{\eta}_A,$$
$$\dot{\varepsilon}^{Tph} = \dot{\varepsilon}_C^{Tph} = \sum_{k=1}^{k=5}\alpha_k\eta_k\dot{T} + \sum_{k=2}^{k=5}\varepsilon_k^{ph}\dot{\eta}_k \qquad (3.5)$$

where: $\alpha_k = \alpha_k(T)$ are coefficients of thermal expansion of: austenite, bainite, ferrite, martensite and pearlite, respectively, ε_A^{ph} (ε_1^{ph}) is the isotropic strains accompanying transformation of the input structure into austenite, whereas ε_k^{ph} are isotropic strains from phase transformation of: austenite into bainite, ferrite, martensite, or of austenite into pearlite, respectively.

The methods for calculation of the fractions of the phases created referred to above were used for carbon tool steel of chemical compositions given in the table 1 [15,17]:

TABLE 1

Chemical composition of test steels

Steel	C%	Mn%	Si%	P%	S%	Cr%	Ni%	Mo%	Cu%
C80U	0,84	0,19	0,21	0,006	0,003	0,11	0,08	0,03	0,14

In order to confirm the accuracy of the phase transformation model dilatometric tests were carried out on the samples of the steel under consideration. The model was verified by comparing the dilatometric curves received for different cooling paces with simulation curves. On the basis of the analysis of the results a slight move of CCT diagram was made in order to reconcile the initiation time of the simulation transformation and the times obtained in the experimental research.

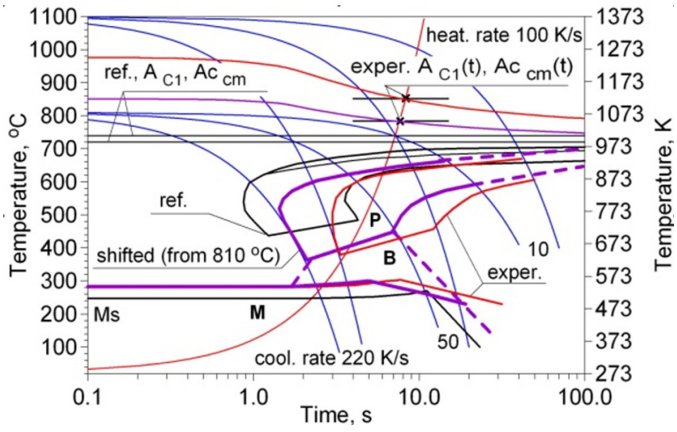

Fig. 2. Diagram CCT with CHT curves for considered steel

Using the results of the tests carried out and the CCT diagram as well as the literature CCT diagram for the steel in question, the CCT diagram was shifted for the purpose of numerical simulations of phase transformation kinetics. Displacement graph obtained from the test result is created in the numerical algorithm that the cooling process the temperature is tracked $T(t_{cool} = 0) = 810°C$). This assumption was based on literature data. The recommended austenitizing temperature for the steel considered is ~810°C [16]. It was assumed that the type of structure obtained in the hardening process depends on the cooling rate starting from the equilibrium temperature Ac_{cm}, and the curve of the beginning of the appropriate transformation. It gives the possibility of using one CCT diagram for different ("substantiation") austenitizing temperatures. These moves were presented, for example, in the studies [15], Fig. 2. After analyzing of the above diagrams it can be noticed that steel under consideration does not contain ferrite but can contain remnant cementite. The curves of CCT diagrams are introduced into a relevant module of phase fraction determination with sup-

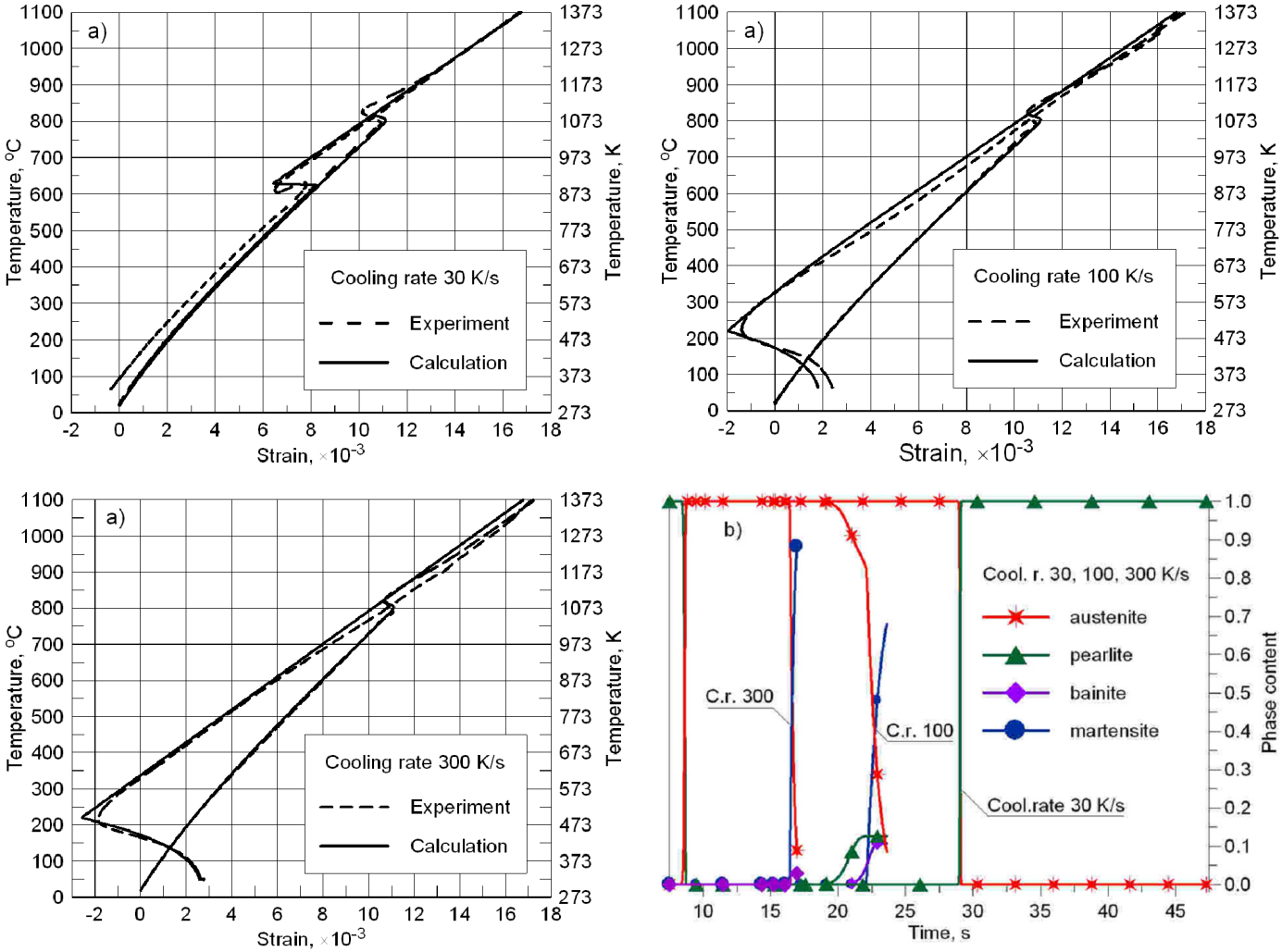

Fig. 3. Experimental and simulation dilatometric curves (a) and kinetics of individual transformation, cool. rate 30, 100 and 300 K/s (b)

Fig. 4. Steel microstructure – zoom × 1000, cool. rate 30, 100 and 300 K/s

plementary information regarding maximum participation of each phase. By using the formulated model of kinetics regarding phase transformations in the solid state, a computer program was built to simulate phase transformations. In order to verify the said program we carried out numerical simulations pertaining to the heating and cooling of an element from carbon tool steel, and then we compared the obtained findings with the findings from dilatometric research [15].

Findings of test simulations are given in figures 3. Due to the fact that in the scope of cooling rate 10÷30 K/s significant changes in the obtained structure were not observed, we only presented findings with respect to 30 K/s. The cooling rate 100 and 200 K/s also was not characterized by significant changes in the obtained structure, hence only the findings with respect to the cooling rate 100 and 300 K/s were presented. By analyzing the obtained findings one may notice that after low cooling rates the considered steel has a perlitic structure (Fig. 3). While the cooling rate increases, the fraction of bainite increases at the expense of declining perlite. However, after high cooling rates – it has martensitic-bainitic or martensitic structure (Figs

3a and 3b). The dilatometric curve obtained from the sample cooled at the rate 100 K/s almost does not exhibit diffusive transformations in the upper temperature range (only traces), and austenite is transformed into bainite (from the temperature ~300°C), and then into martensite (from the temperature M_s). After sample cooling at the rate of 300 K/s, the fraction of martensite is at the level of ~90%, and the rest (~10%) constitutes the retained austenite (Fig. 3b). On the basis of the analysis of simulation and dilatometric curves the values of the thermal expansion coefficient (α_k) and isotropic structural deformations of each structural component $\left(\varepsilon_k^{ph}\right)$ were specified. These coefficients are: 22, 10, 14.5, 10 and 14.5 ($\times 10^{-6}$) [1/K] and 1.0, 4.5, 1.5, 8.7 and 1.5 ($\times 10^{-3}$). It was adopted that 1,2,3,4 and 5 refer to austenite, bainite, ferrite, martensite and pearlite, respectively.

Coefficient of thermal expansion the pearlite structure for considered steel is dependent on temperature (Figs 3a), approximate this coefficient by square function:

$$\alpha_{FP}\left(T\right) = -1.2955\times 10^{-11}T^2 + \\ +2.5232\times 10^{-8}T + 3.7193\cdot 10^{-6} \tag{3.6}$$

4. Mechanical phenomena

In the model of mechanical phenomena, the equilibrium equation without mass forces was adopted in the rate form [2,9,14].

$$\nabla \circ \dot{\boldsymbol{\sigma}}\left(x_\alpha, t\right) = \mathbf{0},\ \ \dot{\boldsymbol{\sigma}} = \dot{\boldsymbol{\sigma}}^T \tag{4.1}$$

where: $\sigma = \sigma(\sigma_{\alpha\beta})$ is a stress tensor, (°) means incomplete internal multiplication factor.

The equations (4.1) are supplemented by constitutive relationships that, if based on an additive model of the rate of strains, will be expressed as follows

$$\dot{\boldsymbol{\sigma}} = \mathbf{E} \circ \left(\dot{\boldsymbol{\varepsilon}} - \dot{\boldsymbol{\varepsilon}}^{Tph} - \dot{\boldsymbol{\varepsilon}}^{p} - \dot{\boldsymbol{\varepsilon}}^{tp}\right) + \dot{\mathbf{E}} \circ \boldsymbol{\varepsilon}^{\mathrm{e}} \tag{4.2}$$

where: $\mathbf{E} = \mathbf{E}(T)$ is a elasticity tensor dependent on temperature (T), $\boldsymbol{\varepsilon}^e$ represents an elasticity strains tensor, $\boldsymbol{\varepsilon}^{Tph}$ isotropic tensor of thermal and structural strains (cf. 3.5), $\boldsymbol{\varepsilon}^p$ plastic strains tensor, whereas $\boldsymbol{\varepsilon}^{tp}$ represents the tensor of transformation plasticity.

The equilibrium equations (4.1) is supplemented with the initial conditions

$$\boldsymbol{\sigma}\left(x_\alpha, t_0\right) = \boldsymbol{\sigma}_0\left(x_\alpha\right) = \mathbf{0},\quad \boldsymbol{\varepsilon}^e\left(x_\alpha, t_0\right) = \boldsymbol{\varepsilon}_0\left(x_\alpha\right) = \mathbf{0} \tag{4.3}$$

and the boundary conditions on parts of the boundary (Γ) is remove the degrees of freedom, i.e.:

$$\dot{\mathbf{U}}\left(x_\alpha, t\right)\big|_{\Gamma_u} = \dot{\bar{\mathbf{U}}},\ \left(\dot{\mathbf{U}}\left(x_\alpha, t\right)\big|_{\Gamma_u} = \mathbf{0}\right) \tag{4.4}$$

where: $\mathbf{U}$ is a displacement vector.

To mark plastic strain the non-isothermal plastic law of flow with the isotropic strengthening and condition plasticity of Huber-Misses and isotropic or kinematic strengthening were used. Functions of plastic flow ($f = f(\sigma, Y)$) adopted so as:

$$f = \sigma_{ef} - Y\left(T, \sum \eta_k, \varepsilon_{ef}^p\right) = 0,$$
$$f = \sigma_{ef} - Y_0\left(T, \sum \eta_k\right) = 0 \tag{4.5}$$

where: σ_{ef} is effective stress, ε_{ef}^p effective plastic strain, $Y = Y(T, \Sigma\eta_k, \varepsilon_{ef}^p)$ is a plasticized stress of material on the phase components $\Sigma\eta_k$ at a temperature T and plasticizing ε_{ef}^p, $Y_0 = Y_0(T, \Sigma\eta_k)$ is a yield points.

Yield stress, in the case of the material model with the isotropic strengthening, is determined a linear function:

$$Y\left(T, \sum \eta_k, \varepsilon_{ef}^{\mathrm{p}}\right) = Y_0\left(T, \sum \eta_k\right) + Y_H\left(T, \sum \eta_k, \varepsilon_{ef}^{\mathrm{p}}\right),$$
$$Y_0\left(T, \sum \eta_k\right) = \sum Y_0^k\left(T\right)\eta_k \tag{4.6}$$

where: Y_H is the surplus of the yield strength resulting from the strengthening of the material.

Plastic strains are determined by the associated theory of plastic flow [11,17]:

$$\dot{\boldsymbol{\varepsilon}}^p = \dot{\Lambda}\frac{\partial f}{\partial \boldsymbol{\sigma}},\quad \dot{f} = 0,\quad f = 0,$$
$$\dot{\boldsymbol{\varepsilon}}^p = \dot{\Lambda}\frac{3\mathbf{S}}{2Y}\ \ \text{or}\ \ \dot{\boldsymbol{\varepsilon}}^p = \dot{\Lambda}\frac{3}{2}\frac{\mathbf{S}-\boldsymbol{\alpha}}{Y_0} \tag{4.7}$$

where: Λ is a plasticity scalar multiplication factor, $\mathbf{S}$ represents a deviator of stress tensor ($\mathbf{S} = \boldsymbol{\sigma} - \mathbf{I}\sigma_{kk}/3$), a is a tensor of displacement of the centre of plastic flow surface (in model with kinematic strengthening).

To investigate transformation plasticity, the modified Leblond equation was used in which a function decreasing the rate of transformation plasticity with the time of transformation was applied [3], i.e., for isotropic or kinematic strengthening:

$$\dot{\boldsymbol{\varepsilon}}^{tp} = 0,\ \eta_k < 0.03,\ \dot{\boldsymbol{\varepsilon}}^{tp} = \\ \begin{cases} -\dfrac{\mathbf{S}}{Y_1}\sum_{k=2}^{k=5}\left(1-\eta_k\right)K_{1k}\ln\left(\eta_k\right)\dot{\eta}_k, \\ \text{or } -\dfrac{\mathbf{S}-\boldsymbol{\alpha}}{Y_{01}}\sum_{k=2}^{k=5}\left(1-\eta_k\right)K_{1k}\ln\left(\eta_k\right)\dot{\eta}_k \end{cases},\ \eta_k \geq 0.03 \tag{4.8}$$

where: $K_{1k} = 3\varepsilon_{1k}^{ph}$ are volumetric structural strains when the material is transformed from the initial phase „1" into k-phase, Y_1 and Y_{01} are plasticized stress and the yield points at the output phase (soft i.e.: austenite).

The problem of thermo-elasto-plasticity is solved by the finite element method, and the modified Newton-Raphson algorithm was used in the iterative process of determining plastic deformation. [14], and the end of the iterative process in the incremental step determined the conditions:

$$\left|\sigma_{ef}^{s+1} - Y^{s+1}\right| \leq \Delta^Y,\quad \left|\sigma_{ef}^{s+1} - Y_0\right| \leq \Delta^{Y_0} \tag{4.9}$$

where: Δ^Y, Δ^{Y_0} they are assumed errors of the completion of the iterative process, they were assumed equal: $\Delta^Y = 10^{-3}\times Y(T, \Sigma\eta_k)$, $\Delta^{Y_0} = 10^{-3}\times Y_0(T, \Sigma\eta_k)$.

5. Example of calculations

On the basis of the presented models pertaining to hardening phenomena we built a computer program to simulate hardening phenomena. By using this program a numerical simulation was carried out with respect to the progressive hardening of a carbon tool steel element. The initial structure was perlite (spheroidite). An axially symmetric object (shaft), 25 mm in diameter, was subjected to the simulation. A control area equal to $h = 120$ mm was adopted. It was assumed that from the coordinate $z = h$ to the coordinate $z = h + h_\infty = 250$ mm temperature changes linearly to the temperature of the cooling medium (T_∞). Dimensions, source location, intensive cooling zone, and boundary conditions for the thermal conductivity equation are presented in figure 5.

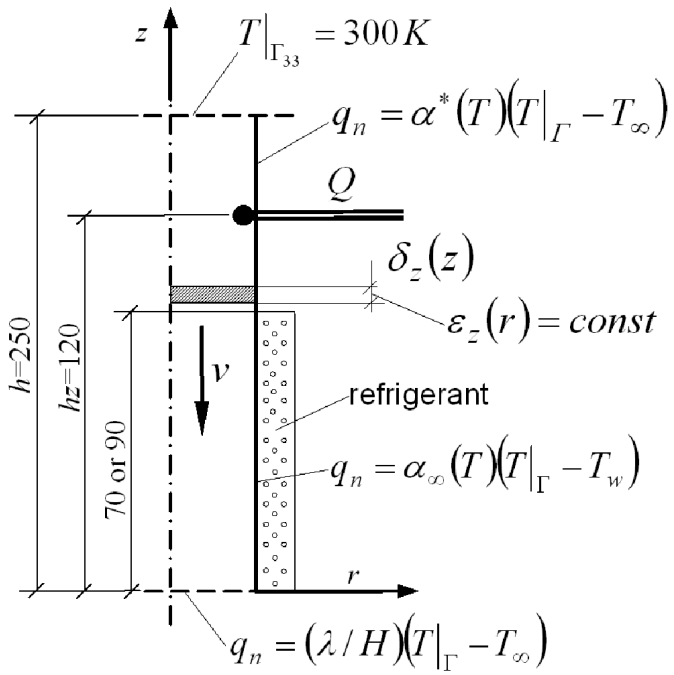

Fig. 5. Diagram of the considered system and adopted boundary conditions

Surface layer heating was carried out by means of the volume source (simulating induction heating [17]) on the length of 10 mm to the depth of 2 mm from the outer surface. Thermophysical coefficients appearing in the conductivity equation (λ,ρ and c) were adopted as constant. Their values, calculated on the basis of data given in the works [2,9], were equal to: $\lambda = 35$ W/(mK), $\rho c = 5.5\times10^6$ J/(m^{3}K), respectively. The cooling was carried out by the flux resulting from temperature differences between the side surface and the cooling medium (Newton boundary condition). Two lengths of the cooling zone were assumed, equal to 70 or 90 mm (Fig. 7)). Temperatures: initial of the object (T_0) and of the cooling medium ($T\infty$) were adopted as equal to 300 K. The heat transfer coefficient in the spray zone was constant, equal to 4200 W/(m^{2}K). In the open zone, the heat transfer coefficient, with the radiation (α_r) (cf. 2.5) was adopted with the value 50 W/(m^{2}K). The adjustment rate of the object, in the control area, was equal to 36 m/hour. The force of the heating source, which ensured maximal temperature on the surface ≈1500 K with respect to the assumed rate (Figs 6 and 7), was determined to be 1.4 kW. It resulted in force density (Q in the equation (2.1)) equal to 9.7×10^8 W/m^3, in the area of source activity. In the simulation of thermal phenomena, the heat of phase transformation was not considered due to the excessively small area heated above the temperature Ac_1 (Fig. 6), heat of phase transitions was not taken into account. Temperature distributions, obtained from the simulation after the determination of the heating process, are presented in figures 6 and 7.

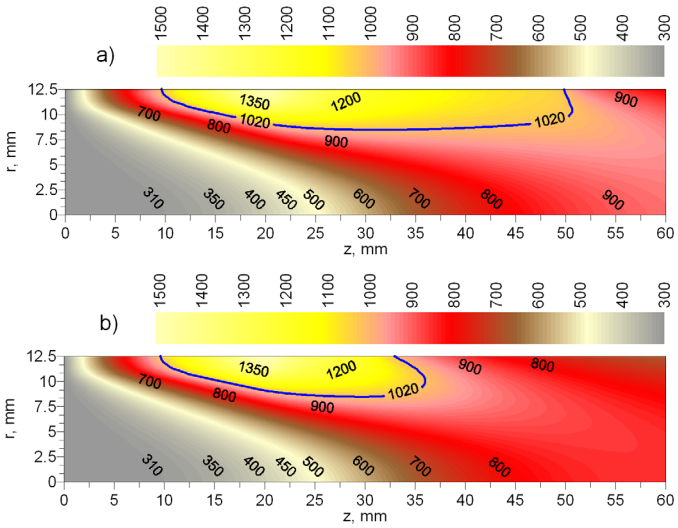

Fig. 6. Temperature distributions in longitudinal section of hardened object, a) cooling the length of 70 mm, b) cooling the length of 90 mm

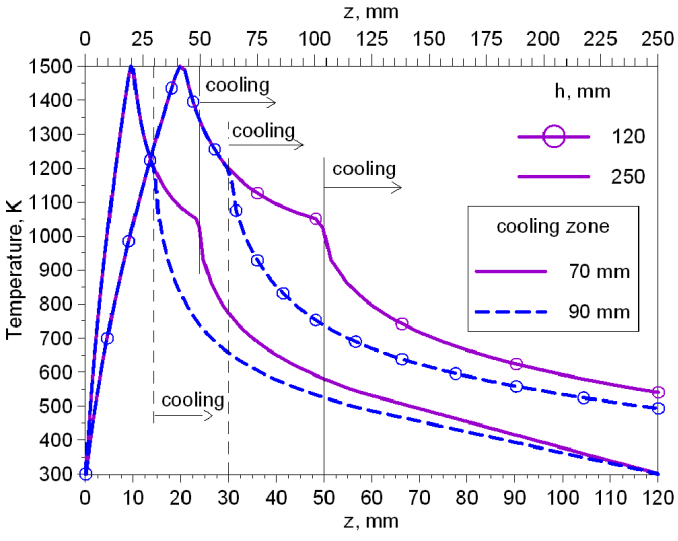

Fig. 7. Temperature distribution on a side surface of the hardened object

After object heating we carried out a simulation of phase transformation and mechanical phenomena determining the fractions of phases, plastic strains and stresses. In the simulation of phase transformation into austenite, CHT diagram was used, i.e., curves $Ac_1(t)$ and $Ac_{cm}(t)$ (see Fig. 2). Distributions of particular phases obtained from the simulation of phase transformations, transformation kinetics in the surface layer and the history of

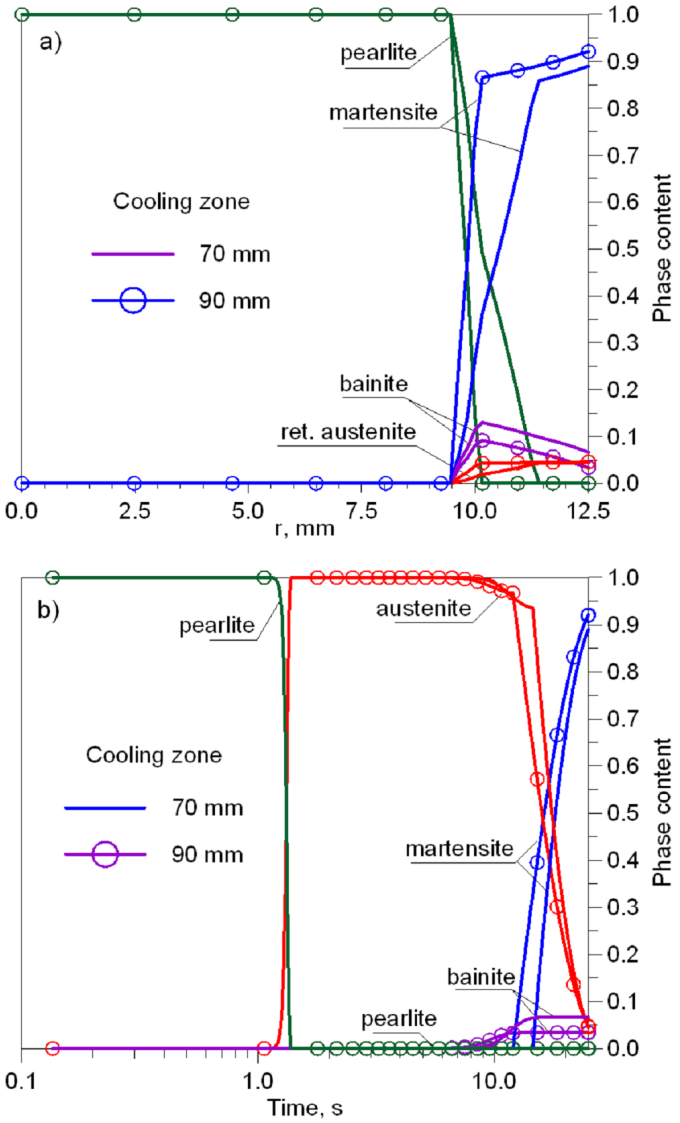

Fig. 8. Phases fractions, a) distributions along the radius, b) the kinetics of transformations in boundary layer

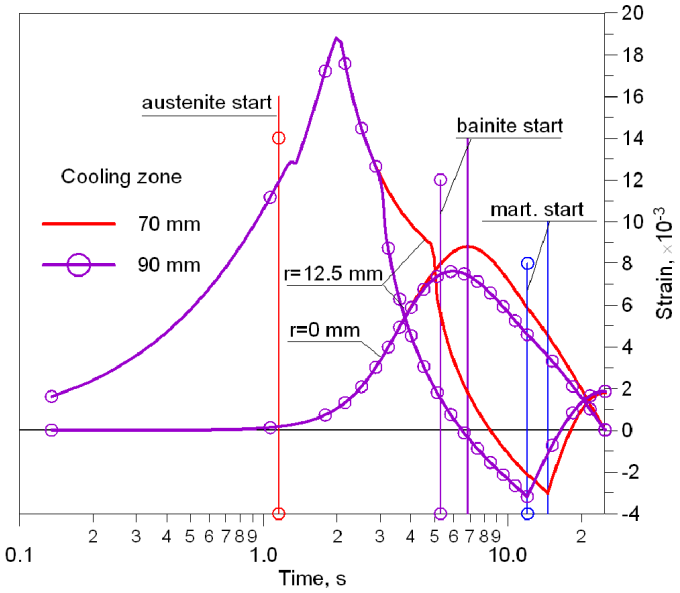

Fig. 9. The history of generating isotropic thermal and structural strains (ε^{Tph}) in the core and in the surface layer (Fig. 5)

thermal and structural strain generation, are presented in figures 8 and 9, respectively.

In the simulation of mechanical phenomena, the Young's modulus and the tangential modulus was dependent on temperature, whereas the yield point – on temperature and phase composition of the object. Young's modulus and tangential modulus (E and E_t) were equal to $E = 2\times10^5$ and E_t=1,1×10^3 [MPa] ($E_t = 0{,}055E$), respectively, whereas the yield point ($Y_{0(.)}$): 150, 450, 1100 and 300 [MPa], for austenite, bainite, martensite, and perlite (ferrite), respectively, at the temperature 300 K. At the solidus temperature (1700 K) and higher, the Young's modulus and tangential modulus were adopted with values 100 and 5.5 [MPa], whereas yield points were equal to 5 [MPa]. These values were adopted on the basis of data given in the works [2,9]. The assumed values of the Young's modulus, tangential modulus and yield point for perlite (spheroidite), at the temperature 300 K, confirm the findings obtained from the static tensile test of the sample from the considered steel. By using discrete values of thermophysical sizes dependent on temperature it was possible to carry out approximation thereof by means of square spline functions (tangents for the temperature argument T_{tn}) to obtain the following approximation polynomials (temperature in Kelvin degrees).

– for Young's modulus and tangent module [MPa], $T_{tn} = 970$ K

$$E(T) = \begin{cases} 2.0\times10^5, & T < 300\,\text{K} \\ \sum_{j=0}^{j=2} a_j T^j, & T \in [300,\ T_{tn} = 970] \\ \sum_{j=0}^{j=2} b_j T^j, & T \in (T_{tn} = 970,\ 1700] \\ 100, & T > 1700\,\text{K} \end{cases},$$

$$E_t(T) = 0.055 \cdot E(T) \qquad (5.1)$$

where:
a_j = (1.8394E+0005, 1.0709E+0002, –1.7848E-0001),
b_j = (6.8785E+0005 –8.0912E+0002, 2.3798E-0001),
j = 0,1,2.

– for yield points $Y_0(T_0, \eta_k)$ [MPa] (k = 1,2,3,4,5 for austenite, bainite, ferrite, martensite and perlite, respectively), T_{tn} = 900 K

$$Y_0(T, \eta_k) = \begin{cases} Y_0(T_0, \eta_k), & T < 300\,\text{K} \\ \sum_{j=0}^{j=2} a_j^{(k)} T^j, & T \in [300,\ T_{tn} = 900] \\ \sum_{j=0}^{j=2} b_j^{(k)} T^j, & T \in (T_{tn} = 900,\ 1700] \\ 5, & T > 1700\,\text{K} \end{cases} \qquad (5.2)$$

where:
$a_j^{(1)}$ = (1.3446E+0002, 1.0357E–0001, –1.7262E–0004),
$b_j^{(1)}$ = (3.7915E+0002, –4.4018E–0001, 1.2946E–0004),

$a_j^{(2)}$ = (4.0232E+0002, 3.1786E–0001, –5.2976E–0004),
$b_j^{(2)}$ = (1.1533E+0003, –1.3509E+0000, 3.9732E–0004),
$a_j^{(3)}$ = (2.6839E+0002, 2.1071E–0001, –3.5119E–0004),
$b_j^{(3)}$ = (7.6621E+0002, –8.9554E–0001, 2.6339E–0004),
$a_j^{(4)}$ = (1.0273E+0003, 8.1786E–0001, –1.3631E–0003),
$b_j^{(4)}$ = (2.9595E+0003, –3.4759E+0000, 1.0223E–0003),
$a_j^{(5)} = a_j^{(3)}$, $b_j^{(5)} = b_j^{(3)}$, $j = 0,1,2$.

Due to the complicated geometry of the object and the manner of its hardening (progressive hardening), we used the equilibrium equation in polar coordinates. Constitutive relationships adopted for the modified plane state of strain ($\dot{\varepsilon}_{33}(x_3) = \dot{\varepsilon}_z(z) \neq 0$) fulfilling the integral conditions:

$$\int_{\Gamma_{33}} \dot{\sigma}_{33} d\Gamma = 0 \quad \text{and} \quad \int_{\Gamma_{33}} \dot{\sigma}_{33} d\Gamma = \dot{N}\big|_{\Gamma_{33}} \neq 0 \qquad (5.3)$$

where: N is the resultant normal force acting in cross-section G_{33} (in cross-section perpendicular to the axis $z = x_3$) (see Fig. 5), coming from the boundary conditions (in cases of conditions ensuring external static determination it is equal to zero).

In the simulation of mechanical phenomena, with the assumption regarding the modified plane strain state and normal resultant force zeroing ($N = 0$) in the cross-section of the object (Γ_{33}). Therefore, it was assumed that in a given shaft ring with differential thickness $\delta_z = \delta_z(z)$ (Fig. 5), due to the circumferential symmetry of heat load and from phase transformations, the total strains on the direction perpendicular to the cross-section are different from zero, (independent from the radius $\varepsilon_z(r) = \text{const}$), i.e., $\dot{\varepsilon}_{33} = \dot{\varepsilon}_z(z)$. These strains are determined by the integral equation (5.3):

After using the constitutive relationship for σ_{33} [14] and substitution to (5.3) gives the formula for $\dot{\varepsilon}_z(z)$:

$$\dot{\varepsilon}_z(z) = \begin{pmatrix} -\int_r \lambda(\dot{\varepsilon}_r^e + \dot{\varepsilon}_\phi^e) r dr + \\ -\int_r \left(2\dot{\mu}\varepsilon_z^e + \dot{\lambda}\varepsilon_{\alpha\alpha}^e\right) r dr \end{pmatrix} \Bigg/ \int_r (2\mu + \lambda) r dr +$$
$$+ \int_r (2\mu + \lambda)\left(\dot{\varepsilon}_z^p + \dot{\varepsilon}_z^{tp} + \dot{\varepsilon}^{Tph}\right) r dr \Bigg/ \int_r (2\mu + \lambda) r dr,$$
$$\alpha = 1,2,3 \qquad (5.4)$$

where: $\lambda = \lambda(E(T),\nu)$ $\mu = \mu(E(T),\nu)$ are the Lame constants, E is Young's module, ν it is Poisson's ratio.

Unfortunately, non-zero strains in the direction perpendicular to the considered cross-section determined by the dependence (5.4) and inserted into the constitutive relationship (4.2) enforce an additional iterative process. In this iterative process, it was assumed that the termination of iteration is:

$$\left|\varepsilon_z^{i+1} - \varepsilon_z^i\right| \leq \Delta^{\varepsilon_{33}} = 3 \times 10^{-4} \left|\varepsilon_z^i\right| \qquad (5.5)$$

In the iterative process of searching for plastic deformation, the condition (4.9) is generally met in parallel with the conditions (5.5).

The obtained simulation results of mechanical phenomena are presented on the figure 10÷13. Based on the analysis of the results from the simulation of such a hardening method, one can assess it, what influence on the hardening stress that is generated

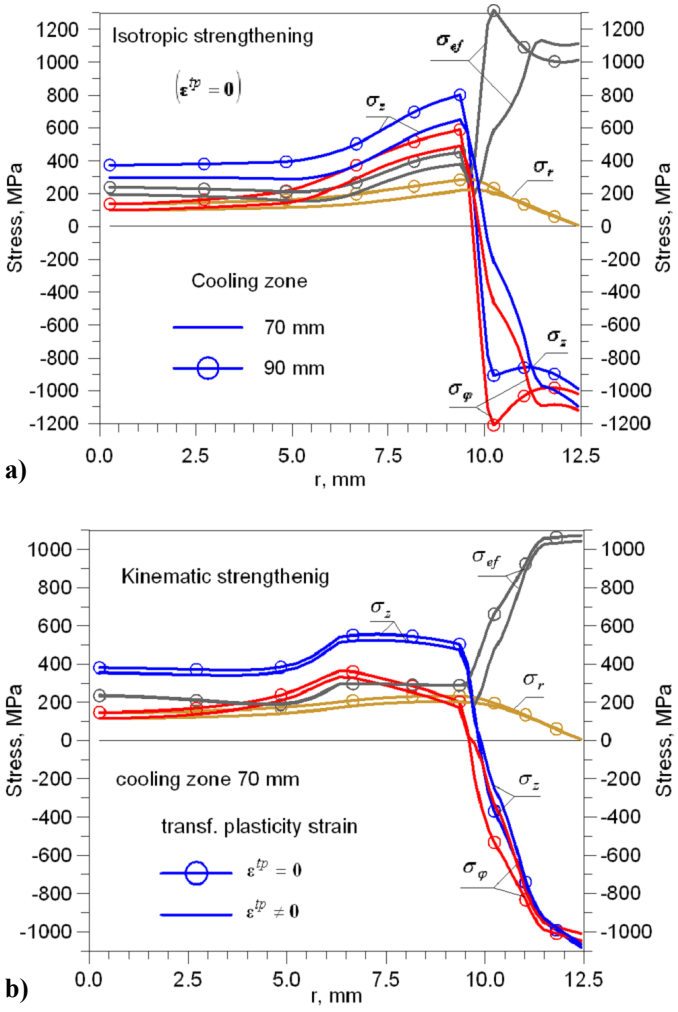

Fig. 10. Distributions of residual stress along the radius. a) influence of length of the cooling zone, b) with and without transformation plasticity

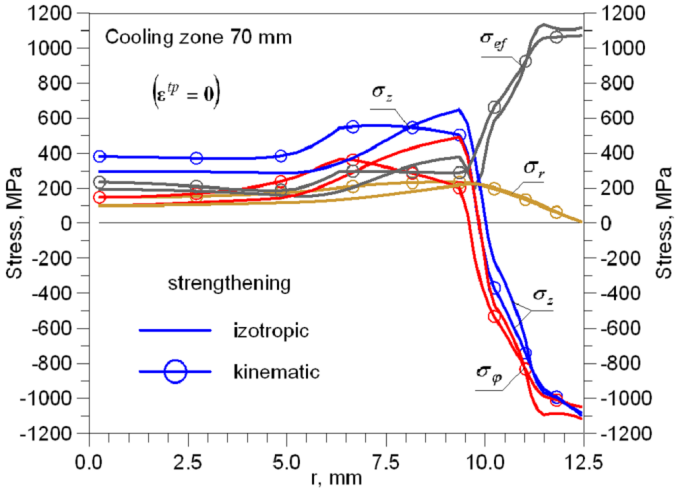

Fig. 11. Distributions of residual stress along the radius. The influence of the type of strengthening

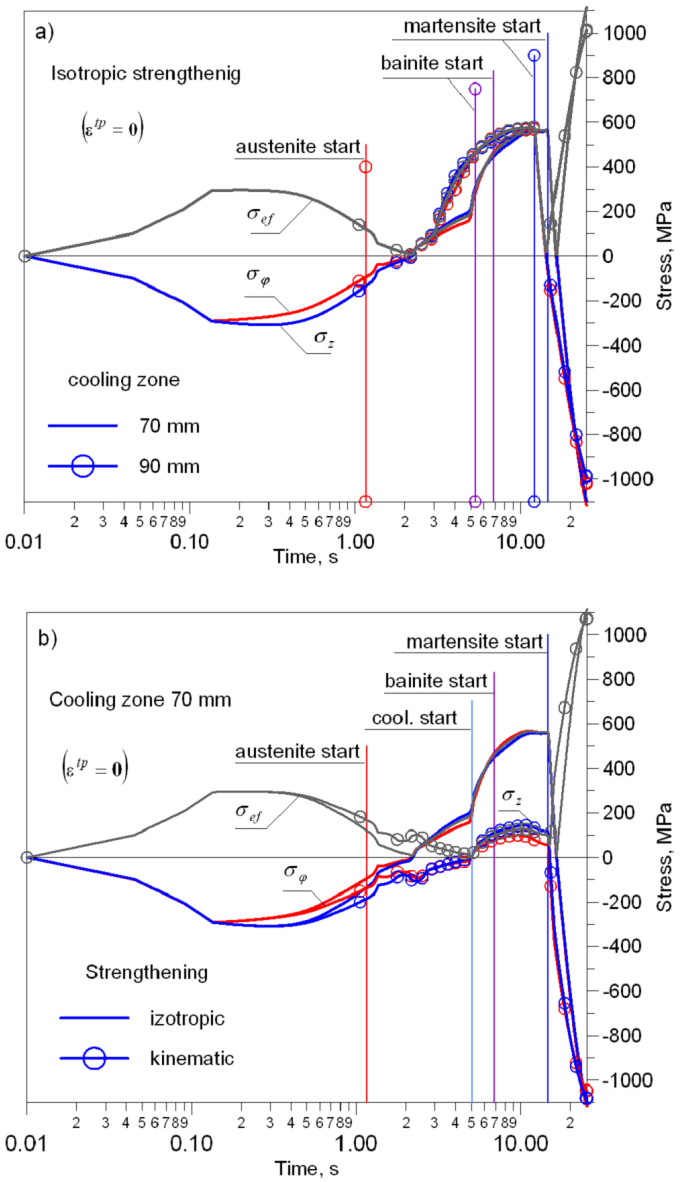

Fig. 12. History of stress generating in the surface layer, a) influence of the cooling zone, b) influence of the type of strengthening

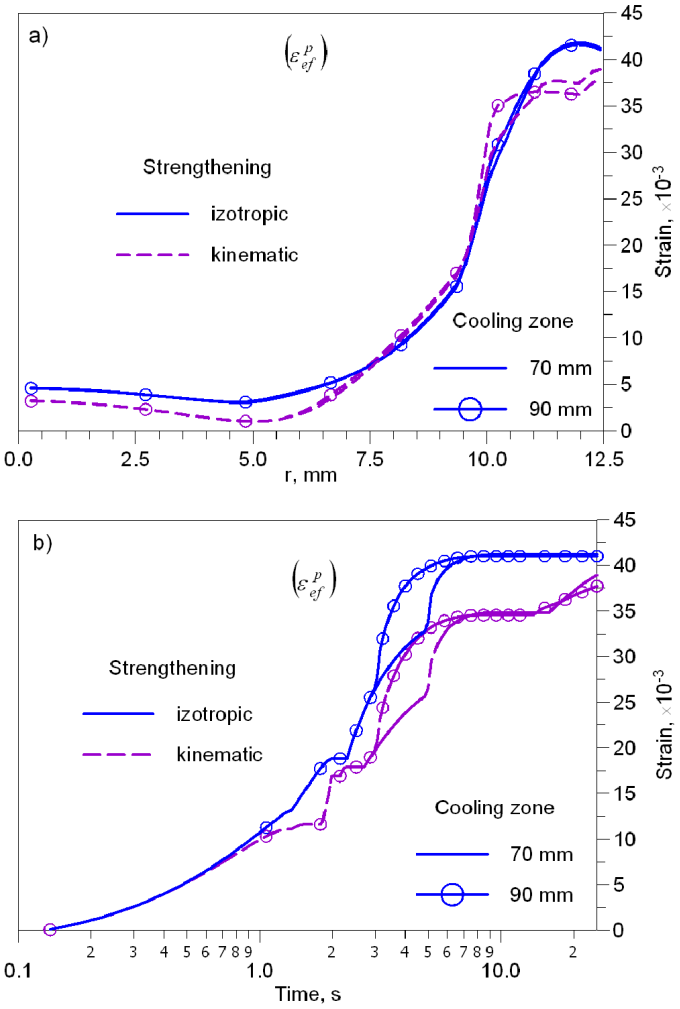

Fig. 13. The effective plastic strain, a) distribution along the radius, b) history of generating strains in the surface layer

is to take into account in the stresses model transformation plasticity, the length of the cooling area and the type of strengthening of the hardened material.

6. Conclusions

During the analysis of findings obtained from the simulation of progressive hardening of the tool steel object, which was heated by means of the movable volumetric heat source, one may observe that after the adoption of the heating and cooling method with respect to the hardened shaft, the retained austenite, bainite and martensite occur only in surface layers (Fig. 8). It means that, already at this stage of the simulation, one may predict a positive distribution of hardening stresses and a positive strengthening zone of the material. Stress distributions after such hardening are very beneficial (Fig. 10,12). In the surface layer, circumferential and axial stresses are compressive. Although the depth of the hardened zone is almost independent from the length of the cooling zone (Fig. 8a), a change of the length of the cooling zone has impact on the hardening stress distribution (Fig. 10a). It occurs due to the influence of a change of generated thermal and structural strains in cooling zones (Fig. 9a) on the generation history of hardening stresses (Fig. 12a).

Even though the impact of transformation plasticity may be omitted in the simulation of progressive hardening of the surface layer heated by the surface volumetric movable heat source, the influence is already noticeable (Fig. 10b). Differences in the stress distributions are also obtained depending on the assumption in the simulation with regard to the material that can have either an isotropic or kinematic strengthening characteristic (Fig. 11). These differences are not significant (despite the significant difference in the stress generation history (Fig. 12b)), but – noticeable because in such a process there are in loading and unloading. It is also observed that in such a hardening method significant plastic strains are generated in the surface layer. Material strengthening appears in surface layers (Fig. 13) meaning that the surface layer after such hardening has good mechanical properties (increased yield point).

REFERENCES

[1] H. Xie, J. Cheng, J. Li, Determination of surface heat-transfer coefficients of steel cylinder with phase transformation during gas quenching with high pressures, Computational Materials Science **29**, 453-458 (2004).

[2] M. Coret, A. Combescure, A mesomodel for the numerical simulation of the multiphase behavior of materials under anisothermal loading (application to two low-carbon steels), International Journal of Mechanical Sciences **44**, 1947-1963 (2002).

[3] L. Taleb, F. Sidoroff, A micromechanical modelling of the Greenwood-Johnson mechanism in transformation induced plasticity, International Journal of Plasticity **19**, 1821-1842 (2003).

[4] B. Chen, X.H. Peng, S.N. Nong, X.C. Liang, An incremental constitutive relationship incorporating phase transformation with the application to stress analysis, Journal of Materials Processing Technology **122**, 208-212 (2002).

[5] F. Fischer, G. Reinsner, E. Werner, K. Tanaka, G. Cailletaud, T.Antretter, A nev view on transformation induced plasticity (TRIP), International Journal of Plasticity **16**, 723-748 (2000).

[6] L. Huiping, Z. Guoqun, N. Shanting, H. Chuanzhen, FEM simulation of quenching process and experimental verification of simulation results, Material Science and Engineering A 452-453, 705-714 (2007).

[7] Ch. Heming, H. Xieqing, W. Honggang, Calculation of the residual stress of a 45 steel cylinder with a non-linear surface heat--transfer coefficient including phase transformation during quenching, Journal of Materials Processing Technology **55**, 339-343 (1999).

[8] D.Y. Ju, W.M. Zhang, Y. Zhang, Modeling and experimental verification of martensitic transformation plastic behavior in carbon steel for quenching process, Material Science and Engineering A 438-440, 246-250 (2006).

[9] S.-H. Kang, Y.T. Im, Three-dimensional thermo-elastic-plastic finite element modeling of quenching process of plain carbon steel in coulee with phase transformation, Journal of Materials Processing Technology 192-193, 381-390 (2007).

[10] W. Piekarska, M. Kubiak, Z. Saternus, Numerical modelling of thermal and structural strain in laser welding process, Archives of Metallurgy and Materials **57** (4), 1219-1227 (2012).

[11] M. Avrami, Kinetics of phase change, Journal of Chemical Physics I vol. 7, 1103-1112, II vol. 8, 1940, 212-224, III vol. 9, 1941, 117-184 (1939).

[12] D.P. Koistinen, R.E. Marburger, A general equation prescribing the extent of the austenite-martensite transformation in pure iron--carbon alloys and plain carbon steels, Acta Metallurgica **7**, 59-60 (1959).

[13] M. Dalgic, G. Löwisch, Transformation plasticity at different phase transformation of bearing steel, Mat.-wiss. u, Werkstofftech **37**, 1, 122-127 (2006).

[14] O.C. Zienkiewicz, R.L. Taylor, The finite element method, Butterworth-Heinemann, Fifth edition **1**, 2, (2000).

[15] T. Domański, A. Bokota, The numerical model prediction of phase components and stresses distributions in hardened tool steel for cold work, International Journal of Mechanical Sciences **96-97**, 47-57 (2015).

[16] J. Orlich, A. Rose, P. Wiest, Atlas zur Wärmebehandlung von Stähle, III Zeit Temperatur Autenitisierung Schaubilder, Verlag Stahleisen MBH, Düsseldorf (1973).

[17] P.M. Pacheco, M.A. Savi, A.F. Camarao, Analysis of residual stresses generated by progressive induction hardening of steel cylinders, Journal of Strain Analysis **36**, 5, 507-516 (2001).